Application of Proper Orthogonal Decomposition Methods in Reactive Pore Diffusion Simulations

Martin Ullmann,[1]* Uwe Prüfert,[2] Jens Seidel,[3] Oliver G. Ernst[3] and Christian Hasse[1]

1. Chair of Numerical Thermo-Fluid Dynamics, TU Bergakademie Freiberg, Fuchmühlenweg 9 09599, Freiberg, Germany

2. Institute of Numerical Analysis and Optimization, TU Bergakademie Freiberg, Akademiestraße 6 09599, Freiberg, Germany

3. Chair of Numerical Mathematics, TU Chemnitz, Raichenhainer Straße 41 09126, Chemnitz, Germany

Reactive pore diffusion is an important process in automotive exhaust-gas aftertreatment modelling the overall conversion of pollutants. It features highly nonlinear source terms from chemical reactions coupled with transport processes. This work examines the application of model reduction by proper orthogonal decomposition. It is shown that this technique can be successfully applied to the system using separate bases for each species. Using a basis obtained for baseline conditions, predictions can be made for species profiles within a pore system for different conditions, potentially leading to significantly reduced computational requirements.

Keywords: catalysis, mathematical modelling, modelling and simulation studies, transport processes

INTRODUCTION

Automotive exhaust-gas aftertreatment systems are complex systems with several processes happening simultaneously at different scales in time and space. A raw exhaust-gas is led through the numerous parallel channels of a ceramic monolith. Within the channel the gas interacts with the channel walls, usually made of a highly porous washcoat layer, exchanging heat and also gaining access to the washcoat's pore system. The reactive precious metal responsible for the conversion of pollutants to less harmful substances is finely dispersed within this pore system. Hence, the gases have to be transported to the active metal sites via diffusion processes and subsequently interact with the surface-bound catalyst. The processes within the washcoat and a single pore are illustrated in Figure 1.

Several methods with varying level of detail can be used to model washcoats. One way is to include all washcoat effects in the kinetics of the chemical reactions itself. Thus, looking at Figure 2, chemical reactions on the catalytic active surface can be directly coupled with the monolith's channel flow without the need for a separate washcoat submodel. It allows for fast computations of a washcoat, which has been characterized sufficiently well to parameterise this simplified physical description. The range of application of this kind of model is limited to the conditions at which the reaction kinetics of the system was determined. These models are not suitable for extrapolation to other temperature or pressure ranges, or changes of the washcoat substrate through aging processes.[1–3]

On the other hand, models with fully three-dimensional resolved pore systems and elementary step kinetics can be applied to a wide range of conditions, albeit at the expense of computational effort.[6–8]

For catalyst simulations involving drive cycle simulations or other large scale applications with a multitude of pore system evaluations, a trade-off between the employed model accuracy and the simulation speed has to be found. For these cases two approaches can be distinguished. On the one hand, a detailed model based on finding the solution of a one-dimensional reaction-diffusion problem with detailed chemistry, on the other hand the so-called effectiveness factor model, based on an analytical solution of the diffusion problem.[9–13]

Although the effectiveness factor model is considered to be one to two orders of magnitude faster than the detailed model, it is only applicable under certain circumstances. These requirements, like first order kinetics or the availability of one representative species describing the behaviour of the entire system, are quite often not satisfied, resulting in unrealistic behaviour of the modelled system. Thus, although it is slower, the model solving a 1D diffusion-reaction equation is the most suitable for catalyst simulations.

In the following, it is examined how reduced order models (ROM) can be applied to this modelling approach to decrease the computational effort associated with the detailed model, while still keeping the high levels of accuracy of the original model. It should be noted that this examination is only a first step towards the applicability of ROM in reactive pore diffusion systems. As always, the application of the model reduction technique comes with certain detriments, for example additional computational steps during the time integration, which will be discussed in the following sections. The success of this technique must be examined on a per case basis, as the trade-off between model reduction and increased computational effort in other places cannot be predicted and is highly dependent on the chemical mechanism and the reaction system of each individual case.

Modelling the Pore System

Species profiles within the washcoat are modelled under the assumption that concentration gradients in the pore system exist only in one spatial dimension, that is the concentration of the species varies along the pore length but not in the radial direction.

*Author to whom correspondence may be addressed.
E-mail address: martin.ullmann@iec.tu-freiberg.de
Can. J. Chem. Eng. 92:1552–1560, 2014

DOI 10.1002/cjce.22018
Published online in Wiley Online Library
(wileyonlinelibrary.com).

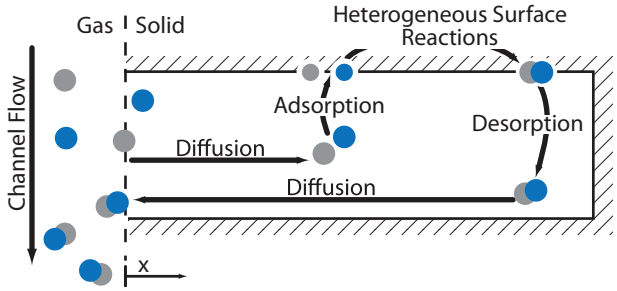

Figure 1. Processes in the washcoat of a catalytic converter.

The time-evolution of the species' concentrations can then be modelled by a set of 1D-reaction-diffusion equations of the form:[14]

$$\frac{\partial c_i}{\partial t} = \frac{\partial}{\partial x}\left(D_{\mathrm{eff},i}\frac{\partial c_i}{\partial x}\right) + \gamma \dot{s}_i. \tag{1}$$

Here, x is the pore length, and c_i and $D_{\mathrm{eff},i}$ denote the concentration and effective diffusion coefficient of species i. $D_{\mathrm{eff},i}$ is set to zero for all surface species. $\dot{s}$ is the chemical source term, and γ denotes the catalytic active surface area per washcoat volume. The boundary conditions for the gas-phase species in this equation are

$$c_i(x=0) = c_{i,0}, \tag{2}$$

$$\frac{\partial c_i}{\partial t}\Big| x = x_{\max} = 0. \tag{3}$$

Equation (2) states that the concentration of the gas-phase species at the pore mouth is equal to the gas concentration of the surrounding atmosphere, which is taken from the flow solution along the catalyst channel. Since the pore is surrounded by solid washcoat material, no gas molecules can pass through the end of the pore. Thus, the diffusive flux at the pore end, and therefore also all concentration gradients for gas-phase species must vanish, as is expressed by Equation (3).

After an appropriate spatial discretization, for example by finite elements or finite differences, Equation (1) is solved by a suitable time integrator until steady-state conditions are reached.[15]

The diffusion coefficient $D_{\mathrm{eff},i}$ is an effective value which takes into account the washcoat properties tortuosity, τ, and porosity, ε. Tortuosity is an empirical quantity that describes the deviation between ideal cylindrical pores and the actual pore shape.[16] Porosity is a measure of the number of pores in the washcoat.[17]

Using the Bosanquet equation,[18] the effective diffusion coefficient can be determined by

$$\frac{1}{D_{\mathrm{eff},i}} = \frac{\tau}{\varepsilon}\left(\frac{1}{D_{\mathrm{knud},i}} + \frac{1}{D_{\mathrm{mol},i}}\right), \tag{4}$$

with $D_{\mathrm{kund},i}$, the Knudsen diffusion coefficient of species, i, and $D_{\mathrm{mol},i}$, its molecular diffusion coefficient at the given temperature.

Modelling Surface Reactions

The state of the catalytic surface is completely described by the temperature T and species surface coverages Θ_i.[9,19] Using elementary step reactions, reaction rates of heterogeneous reactions at the catalytic surface can be expressed as

$$\dot{s}_i = \sum_{k=1}^{K_\mathrm{S}} (\nu''_{ik} - \nu'_{ik}) k_k \prod_{j=1}^{N_\mathrm{G}+N_\mathrm{S}} c_j^{\tilde{\nu}'_{jk}}, \qquad i = 1,\ldots,N_\mathrm{G}+N_\mathrm{S}. \tag{5}$$

Here, $\dot{s}_i$ is the reaction rate of the i-th species, K_s is the number of elementary step surface reactions, ν''_{ik} and ν'_{ik} are the stoichiometric coefficients of the i-th species in the forward or backward reaction, respectively, N_G and N_S are the numbers of gas-phase and surface species, c_j is the molar concentration of species j, and $\tilde{\nu}'_{jk}$ is the reaction order of the j-th species in the k-th reaction. Surface coverage fractions Θ_i must be converted to molar concentrations given the surface site density Γ and their number of occupied surface sites σ_i:

$$\Theta_i = \frac{c_i \sigma_i}{\Gamma}. \tag{6}$$

The rate coefficients k_k, where the index k denotes the current reaction, are defined by a modified Arrhenius expression as a function of the temperature:

$$k_k = A_k T^{\beta_k} \exp\left(-\frac{E_{\alpha,k}}{\mathrm{RT}}\right) \prod_{i\in N_\mathrm{S}} \Theta_i^{\mu_{ik}} \exp\left(\frac{\varepsilon_{ik}\Theta_i}{\mathrm{RT}}\right). \tag{7}$$

In this equation, A is the pre-exponential factor, T is the thermodynamic temperature, E_α is the activation energy, and R is the universal gas constant. Coverage dependencies like attraction or repulsion of surface species are considered in the surface reaction rates with the variables μ_{ik} and $\in_{ik}$. Gas-phase species adsorbing to the catalytic surface are modelled using stick reactions where the rate coefficient is modelled using an initial sticking coefficient S_i^0. It represents the probability of a gas-phase molecule sticking to the solid surface:

$$S_k^{\mathrm{eff}} = S_k^0 \sum_{i\in N_\mathrm{S}} \theta_i^{\nu'_{ik}+\mu_{ik}}, \tag{8}$$

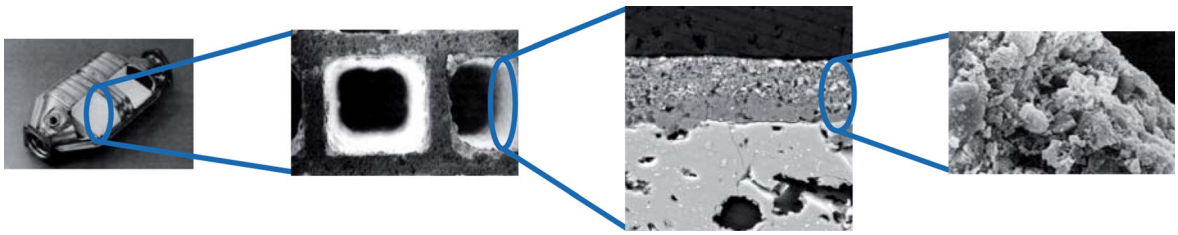

Figure 2. Overview of a three-way catalytic converter. From left to right: the entire device; monolith channels with washcoat; close-up of the porous washcoat; catalytic active surface. Pictures taken from Ref.[4,5]

$$k_k^{\text{stick}} = S_k^{\text{eff}} \sqrt{\frac{RT}{2\pi W_k}}. \tag{9}$$

The mechanism used in this work is a CO-oxidation mechanism on platinum with compressed oxygen submodel taken from Salomons and is shown in Table 1. It consists of four gas-phase, four surface species, and seven reactions.[20]

MODEL REDUCTION WITH POD METHODS

These 1D transient equations describe the physical and chemical processes within the pores. In the simulation of a catalytic converter or a single catalyst channel, this system of differential equations must be solved at each discretization position along the channel. The result of the pore equations influences the species profiles in the channel. Thus, the equations describing the pore system and the catalyst are fully coupled. Especially for larger chemical systems and more complex surface kinetics, this coupled system, and here especially the description of the pore processes, can become computationally very expensive.

One way to reduce time-to-solution of the given reaction-diffusion problem is to reduce the order, that is the number of degrees of freedom, of the system. In this way the model's behaviour can be recreated using fewer state variables than in the full problem above, which leads to a decrease in required CPU time and storage requirements. Here, we will investigate the method of Proper Orthogonal Decomposition (POD), which has been used for different applications such as the analysis of turbulent flows,[21,22] the analysis of engine flows,[23,24] and flows in chemical reactors,[25] as well as reaction-diffusion problems with simple source terms.[26]

General Idea of POD with Time as Snapshot Parameter

We describe the POD method using a general system of partial differential equations:

$$\frac{d}{dt} y(x,t) + \phi(t, y(x,t)) = 0 \text{ in } \Omega \times (0,T), \tag{10}$$

$$\xi(y(x,t)) = 0 \text{ in } \Gamma \times (0,T), \tag{11}$$

$$y(x,0) = y_0 \text{ in } \Omega, \tag{12}$$

where y is a function of a spatial coordinate x and time t, and ϕ is assumed to be separable into linear and nonlinear parts. Obviously, the model equation for the pore system (1) fits this setting. After spatial discretization, for example by finite elements, the semi-discrete problem (13) is obtained.

$$\begin{aligned} M\frac{d}{dt}\boldsymbol{y}(t) + A\boldsymbol{y}(t) + \boldsymbol{F}(t,\boldsymbol{y}(t)) &= 0 \text{ in } (0,T) \\ \boldsymbol{y}(0) &= \boldsymbol{y_0}. \end{aligned} \tag{13}$$

Here, M and A are constant matrices of dimension $N \times N$, and $\boldsymbol{F}$ is a function with $\boldsymbol{F} : \mathbb{R} \times \mathbb{R}^N \to \mathbb{R}^N$. This initial value problem is assumed to have a unique solution.

The state vector $\boldsymbol{y}$ is now replaced by an approximation $\boldsymbol{V}\bar{\boldsymbol{y}} \approx \boldsymbol{y} \in \mathbb{R}^N$, where $\bar{\boldsymbol{y}} \in \mathbb{R}^n$ with $n \ll N$. A reduced order model (ROM) is obtained by multiplying with $\boldsymbol{V}^T$ from the left:

$$\begin{aligned} \boldsymbol{V}^T\boldsymbol{M}\boldsymbol{V}\frac{d}{dt}\bar{\boldsymbol{y}}(t) + \boldsymbol{V}^T\boldsymbol{A}\boldsymbol{V}\bar{\boldsymbol{y}}(t) + \boldsymbol{V}^T\boldsymbol{F}(t, \boldsymbol{V}\bar{\boldsymbol{y}}(t)) &= 0 \text{ in } (0,T) \\ \bar{\boldsymbol{y}}(0) &= \boldsymbol{V}^T\boldsymbol{y_0}. \end{aligned} \tag{14}$$

The columns of $\boldsymbol{V}$ are a set of orthonormal vectors spanning the approximation space of the ROM and are obtained from a given set of solution state vectors associated with different time instants or parameter values, called snapshots in the POD context, by solving the following optimization problem:

$$\min_{\{u_j\}_{j=1}^n} \sum_{i=1}^{i} \left\| \boldsymbol{y}_i - \sum_{j=1}^{n} (\boldsymbol{y}_i^T u_j) u_j \right\|_2^2, \tag{15}$$

subject to

$$u_i^T u_j = \delta_{ij} \quad \forall i,j \in \{1,\ldots,n\}, \tag{16}$$

where δ_{ij} is the Kronecker delta, u are the basis vectors, and l is the number of snapshots.

Equation (13) is solved by a suitable time integrator, for example with a step-size controlled BDF scheme, to obtain a set of solution snapshots $\mathbf{y}_i$, $i = 1, \ldots, l$ of Equation (13) at time t_i. Note that the associated time steps need not be equidistant. The solutions are collected in $\boldsymbol{Y} = [\boldsymbol{y}_1, \ldots \boldsymbol{y}_l] \in \mathbb{R}^{N,l}$.

Finding the solution of Equation (15) is equivalent to finding the left singular vectors of the snapshot matrix $\boldsymbol{Y}$. A singular value decomposition (SVD) yields matrices, such that

$$\boldsymbol{Y} = USV^T, \tag{17}$$

where $U \in \mathbb{R}^{N,N} = [u_1, \ldots, u_N]$ and $V \in \mathbb{R}^{l,l}$. The matrices U and V are orthogonal, that is $V^TV = I_l$ and $U^TU = I_N$. For the given problem, only the left singular vectors u_i, $i = 1,\ldots,l$ are of interest. The matrix $S \in \mathbb{R}^{N,l}$ contains the singular values σ_i of $\boldsymbol{Y}$ with $\sigma_1 \geq \sigma_2 \geq \ldots \geq \sigma_l$. The POD is formed by selecting the first n left

Table 1. Surface reaction mechanism of the CO oxidation on platinum

#	Reaction	A (mole, cm, s)	E_α (kJ/mol)
Adsorption			
(1)	$CO + PT(s) \rightarrow CO(s)$	$S^0 = 8.4 \times 10^{-1}$	
(2)	$O_2 + 2\ PT(s) \rightarrow 2\ O(s)$	$S^0 = 7.0 \times 10^{-2}$	
Surface reactions			
(3)	$CO(s) \rightarrow CO + PT(s)$	1.0×10^{13}	126.4 $\varepsilon_{CO(s)} = +33$
(4)	$CO(s) + O(s) \rightarrow CO_2 + 2\ PT(s)$	3.7×10^{20}	108 $\varepsilon_{CO(s)} = +33$
(5)	$CO + 2\ O(s) \rightarrow CO(s) + OO(s)$	3.7×10^{20}	50
(6)	$CO(s) + OO(s) \rightarrow CO_2 + O(s) + PT(s)$	3.7×10^{23}	115
(7)	$OO(s) + PT(s) \rightarrow 2\ O(s)$	3.7×10^{23}	105

The initial sticking coefficient is denoted with S0. Dependencies on surface coverages are stated below the relevant reactions.

singular vectors with $n \leq l$. The approximation error of representing the snapshots in the reduced basis $\{u_i\}_{i=1,\ldots,n}$ is given by

$$e_n = \sum_{i=1}^{l} \boldsymbol{y}_i - \sum_{j=1}^{n} (\boldsymbol{y}_i^{\mathrm{T}} u_j) u_{j2}^2 = \sum_{i=n+1}^{l} \sigma_i^2. \tag{18}$$

Obviously, the approximation error depends on the choice of the snapshots and the weighting of the individual snapshots. However, with Equation (18), a criterion for choosing n is given. Note that Equation (15) represents only one possible choice of an optimization problem related to POD model reduction. In the FEM context, the inner product of Equation (16) is usually replaced by the finite-dimensional approximation of the L^2 inner product by introducing a weight for the time distances of the snapshots by α_i. In this case we obtain the optimization problem

$$\min_{\{u_j\}_{j=1}^{n}} \sum_{i=1}^{i} \alpha_i \boldsymbol{y}_i - \sum_{j=1}^{n} (\boldsymbol{y}_i^{\mathrm{T}} M u_j) u_{j2}^2, \tag{19}$$

subject to

$$u_i^{\mathrm{T}} M u_j = \backslash delta_{ij} \qquad \forall i, j \in \{1, \ldots, n\}.$$

When using a uniform spatial mesh and taking snapshots at equidistant times this is only a scaling of Equations (15) to (16). For a more detailed discussion of SVD and POD, we refer to the Golub and Van Loan text.[27]

Modified POD Basis

In many technical applications, Equation (10) represents a system of equations. In our case the vector y consists of the concentrations of the eight involved species. In general, the POD method stays applicable in this case. However, the components of such systems often differ significantly in their dynamics, as is the case for the pore diffusion-reaction problem. Here, some components could be underrepresented in the basis obtained by POD. To overcome this misrepresentation a POD basis is computed for each component separately. The matrix U is now a block-diagonal matrix in which the diagonal blocks contain the individual POD basis for each component.

Handling of the Non-Linearity

Using the basis U of left singular vectors obtained by SVD and using Equation (18) to select a subset $V = [u_1, \ldots, u_n]$ to satisfy a suitable error bound, the following ROM is obtained:

$$\begin{aligned} \boldsymbol{V}^{\mathrm{T}} \boldsymbol{M} \boldsymbol{V} \frac{\mathrm{d}}{\mathrm{d}t} \bar{\boldsymbol{y}}(t) + \boldsymbol{V}^{\mathrm{T}} \boldsymbol{A} \boldsymbol{V} \bar{\boldsymbol{y}}(t) + \boldsymbol{V}^{\mathrm{T}} \boldsymbol{F}(\boldsymbol{V} \bar{\boldsymbol{y}}(t)) &= 0 \text{ in } (0, T) \\ \bar{\boldsymbol{y}}(0) &= \boldsymbol{V}^{\mathrm{T}} \boldsymbol{y}_0. \end{aligned} \tag{21}$$

Assuming that V has n basis vectors, the matrices $V^{\mathrm{T}}MV$ and $V^{\mathrm{T}}AV$ have dimensions $n \times n$, but are usually non-sparse. This is contrary to the sparse matrices resulting from discretizing the differential operator in Equation (13). The non-linear source term $\boldsymbol{F}(V\bar{y}(t))$ is evaluated in the original space, that is the state of the ROM $\bar{y}$ needs to be transformed back into the original space dimension N by $V\bar{y}$ and evaluated in the larger space $\mathbb{R}^N$. From the point of computational efficiency this may be sub-optimal. Here, techniques such as the Discrete Empirical Interpolation Method (DEIM) are available, but the application of DEIM must be discussed on a per case basis. For a deeper discussion on this topic see, for example, Buffoni and Willcox[28] and Chaturantabut and Sorensen.[29] On the other hand, in many cases the effort to evaluate $\boldsymbol{F}(V\bar{y}(t))$ is negligible compared to the effort to evaluate the Jacobian $D\Phi(\bar{y}(t))$. Evaluating the Jacobian several times becomes necessary when solving Equation (21) with implicit time stepping schemes, which are usually required to achieve efficient and accurate solutions for such stiff problems. The Jacobian of the right hand side of the ODE $\Phi := \boldsymbol{V}^{\mathrm{T}} A V \bar{y}(t) + \boldsymbol{V}^{\mathrm{T}} \boldsymbol{F}(V\bar{y}(t))$ is given by

$$D\Phi = \boldsymbol{V}^{\mathrm{T}} \boldsymbol{A} \boldsymbol{V} + \frac{\mathrm{d}}{\mathrm{d}\bar{\boldsymbol{y}}} \boldsymbol{V}^{\mathrm{T}} \boldsymbol{F}(\boldsymbol{V} \bar{\boldsymbol{y}}(t)). \tag{22}$$

Computing $D\Phi$ numerically requires the evaluation of n^2 partial derivatives, for example by finite differences, since $D\Phi$ is, in general, a full matrix. Fortunately, the sparsity pattern of $DF(V\bar{y}(t))$ can often be determined in advance. Since

$$\frac{\mathrm{d}}{\mathrm{d}\bar{\boldsymbol{y}}} \boldsymbol{V}^{\mathrm{T}} \boldsymbol{F}(\boldsymbol{V} \bar{\boldsymbol{y}}(t)) = \boldsymbol{V}^{\mathrm{T}} D\boldsymbol{F}(\boldsymbol{V} \bar{\boldsymbol{y}}(t)) \boldsymbol{V}, \tag{23}$$

it is possible to take advantage of the sparse structure of the Jacobian $DF(V\bar{y}(t))$.

In the given application of pore reaction-diffusion systems, DF is very sparse so that the effort to compute the Jacobian of the unreduced system is much smaller than the effort required to calculate the full Jacobian of the ROM. Specifically, the computation of the right-hand side of Equation (23) needs two additional matrix multiplications with V^{T} and V. Thus, the calculation of $D\Phi$ requires, in addition to the evaluation of the sparse Jacobian, the expansion of the full state vector from the columns of V as well as two matrix-matrix products.

Application to the Pore Problem

The above discussed model reduction strategy was applied to a typical pore diffusion problem defined in Table 2.[11,13] A sample pore was spatially discretized with 200 nodes on an equidistant grid. The reaction considered was an 8-species mechanism for the CO-oxidation on platinum, one of the major processes in exhaust-gas aftertreatment systems. One challenge is to choose the right parameters for the simulation to obtain a good POD basis that sufficiently covers the system dynamics. Very important is the choice of the spatial discretization since the mesh must be fine enough to resolve all modes. In general, the structure of the modes is unknown, such that we chose a rather fine spatial mesh. On the other hand, a fine mesh leads to a more expensive transformation, cf. Equation (21).

Table 2. Properties of the pore system

Property	Unit	Value
Length	μm	100
Diameter	nm	10
Porosity ε		0.4
Tortuosity τ		3
Nodes		200
γ		1.5×10^5
Γ	Mole/cm^2	2.72×10^{-5}
λ		0.8…1.2
δ		0…1

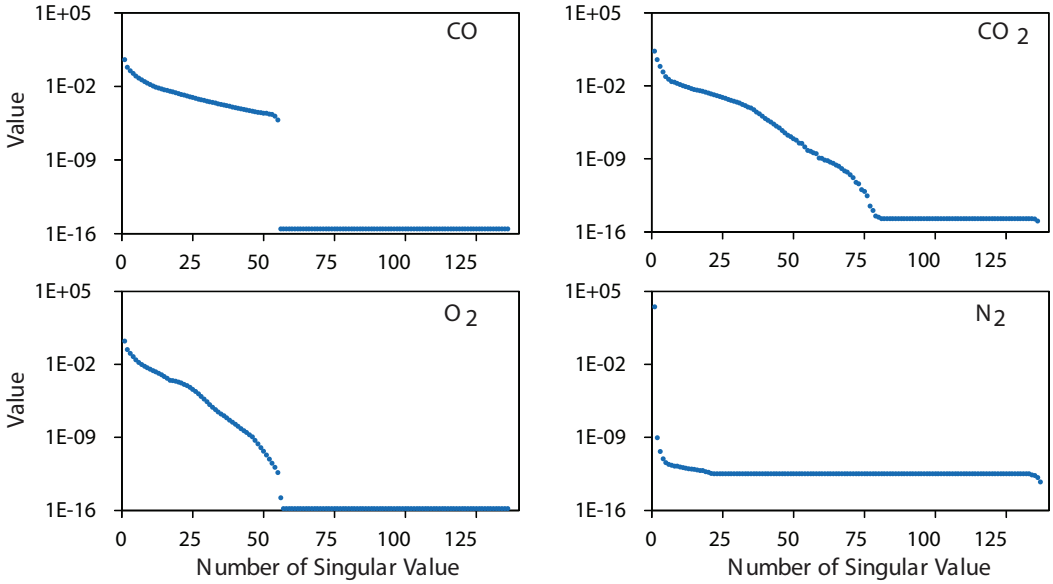

Figure 3. Singular values of the gas-phase species.

Due to interactions of surface species as they are typical for three-way catalysts (see for example reaction of Equations (3) and (4)) the system becomes stiff, meaning that the time scales of the problem can span multiple orders of magnitude, and this must be treated accordingly when integrating in time.

The inlet concentration was varied based on a carrier gas of nitrogen with a baseline concentration of $C^0_{CO} = 8000\,\text{ppm}$. To account for various inlet concentrations of the gas-phase species, the amount of oxygen was varied with the equivalence ratio λ according to

$$C_{O_2} = 0.5 \cdot \lambda \cdot C_{CO}. \tag{24}$$

The conversion along a channel in a three-way catalyst was considered by introducing a conversion factor δ:

$$C_{CO_2} = \delta \cdot C^0_{CO}. \tag{25}$$

$$C_{CO} = (1 - \delta) \cdot C^0_{CO}. \tag{26}$$

Since the surface was assumed to be completely catalytic active platinum at the beginning of each calculation, the composition of the system could be described by using only the two parameters, λ and δ. Note that depending on λ, there can be excess amounts of oxygen or carbon monoxide present that will not be converted, since there is no further reaction partner present in the gas-phase.

Using the model reduction approach for a baseline case with $\lambda = 1$, $\delta = 0$, and at a temperature of 600 K yields singular values as shown in Figures 3 and 4. It can be seen that the largest singular values for each species vary several orders of magnitude, ranging from 3.3×10^3 for N_2 to 3.9×10^{-11} for the compressed oxygen surface species OO(s). This can be explained by the large difference in the molecular concentration of each species. The shown

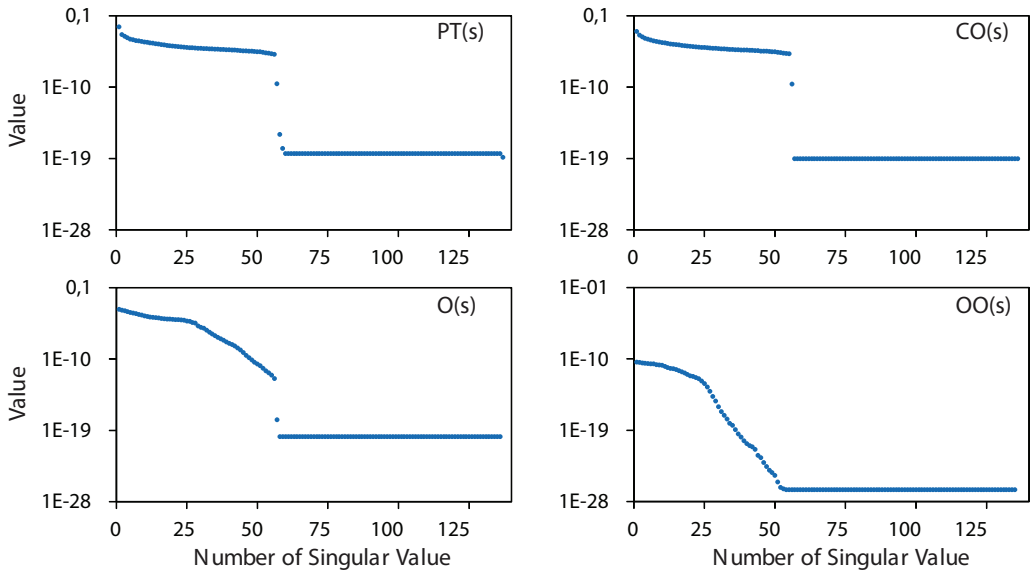

Figure 4. Singular values of the solid species.

behaviour also confirms that an approach treating all species by the same POD basis would lead to a significant under-representation of the minor surface species.

The obtained singular values σ_i decrease slowly for each reactive species. Only N_2 features one distinct value with all others being several orders of magnitude lower. This is due to the fact that N_2 acts as carrier gas and does not take part in the chemical reactions in this case, so that the amount of N_2 in the system stays constant. For all other species, the decrease of the singular values is much slower, which can be especially seen for the surface species. This suggests that the description of the system's behaviour requires a larger number of basis vectors to achieve sufficient accuracy. Using the error criterion given in Equation (18), a suitable number of basis vectors can be obtained for each species. Table 3 shows the number of n basis vectors chosen for each species individually using the error criterion, such that the chosen value is the smallest n that satisfies

$$e_n = \sum_{i=n+1}^{l} \sigma_i^2 < 10^{-10} \cdot \sum_{i=1}^{l} \sigma_i^2. \tag{27}$$

As described earlier, for the source term evaluation the reduced basis needs to be transformed back into the physical space. This transformation introduces a computational overhead that decreases the speed of the POD evaluation. Computation can be accelerated by determining the sparsity pattern of the Jacobian of the system. In the worst case in which, at each grid point, each species influences all others in the chemical source term, the Jacobian would be a sparse matrix consisting of diagonal blocks. The number of blocks in this case would be equal to the number of species in the system and the size of each block equal to the number of spatial grid points, that is in our example 8×8 diagonal blocks of size 200×200. Compared to a full Jacobian, this worst-case sparsity pattern can be computed with only 0.5 % of the function evaluations necessary for the full matrix.

Comparison of the Simulation Results

Using a POD basis created for 600 K, $\lambda = 1$ and $\delta = 0$ simulations were conducted at different conditions and compared to results obtained by solving the system with the standard time integration approach for each condition individually until steady-state conditions were reached. At the given baseline conditions, an absolute cumulated error of 2.50×10^{-7} and relative error of 1.26×10^{-4} could be observed using the ROM. Table 4 shows the errors when using this POD basis for different conditions. The idea is to use one POD basis to cover a large area in the parametric space. Thus, using a small number of tabulated POD bases, the relevant conditions could be simulated. Note that the error shown here is an integral error over the entire system, which means that individual species profiles can deviate significantly from the full model. The errors were determined with the concentration profile from the steady-state solution of the full model c_{full} and the profile from the POD solution C_{POD} to be

$$e_{abs} = ||C_{\text{full}} - C_{\text{POD}}||_2, \tag{28}$$

$$e_{rel} = \frac{||C_{\text{full}} - C_{\text{POD}}||_2}{||C_{\text{full}}||_2}. \tag{29}$$

Deviating further than 10 % from the baseline conditions led to more severe errors. It can be seen that it will not be sufficient to calculate only one POD basis to cover all relevant operating conditions occurring in the system. Instead, several bases spanning multiple baseline conditions will be necessary to have sufficiently accurate results.

Figure 5 and Figure 6 show some obtained steady-state species profiles. While the POD can also predict the transient behaviour, for the problem at hand, only the steady-state solution is of interest. It can be seen that especially surface species are predicted worse for conditions other than the baseline. These species tend to change rapidly depending on the inlet concentrations, for example oxygen surface species become available when λ is larger than 1, as shown above. Since surface species concentrations have large influence on the non-linear source term it is important to predict them within a narrow error margin.

The timing comparison shown in Table 5 suggests that the ROM in average takes slightly less time than the full model.

DISCUSSION OF POD PERFORMANCE

As can be seen in the previous section, the performance of POD ROM is somewhat disappointing. This is mainly caused by the increased computational cost of the evaluation of the Jacobian of the ROM. The number of POD basis vectors needed to meet the error tolerance is 293, resulting in a reduction in degrees of freedom by a factor of $((1600/293) \approx 5.5)$. The timing results displayed in Table 5, however, reveal only modest gains in overall execution time. We attribute this to the dense matrix computations required

Table 3. Number of basis vectors used per species

Species	No. of basis vectors
CO	52
O_2	27
CO_2	32
N_2	1
PT(s)	56
O(s)	42
CO(s)	55
OO(s)	28
Σ	293

Table 4. Error of the POD solution at different conditions for baseline values $T = 600$ K, $\lambda = 1$ and $\delta = 0$

Input value			Absolute	Relative	
T in K	λ	δ	error	error	Remark
600	0.9	0	8.3×10^{-5}	4.2×10^{-4}	λ variation
600	1.1	0	1.0×10^{-5}	5.2×10^{-5}	
600	1.0	0.1	2.1×10^{-5}	1.4×10^{-4}	δ variation
600	1.0	0.2	1.7×10^{-5}	8.4×10^{-5}	
600	1.0	0.3	1.3×10^{-5}	6.6×10^{-5}	
570	1.0	0	1.3×10^{-4}	6.4×10^{-4}	T variation
630	1.0	0	2.1×10^{-5}	1.1×10^{-4}	
600	0.9	0.1	7.8×10^{-5}	3.9×10^{-4}	λ and δ variation
600	1.1	0.1	2.5×10^{-6}	1.3×10^{-5}	
630	1.1	0.1	5.9×10^{-6}	3.1×10^{-5}	λ, δ and T variation
570	0.9	0.1	1.8×10^{-4}	8.8×10^{-4}	
570	1.1	0.1	5.3×10^{-6}	2.6×10^{-5}	

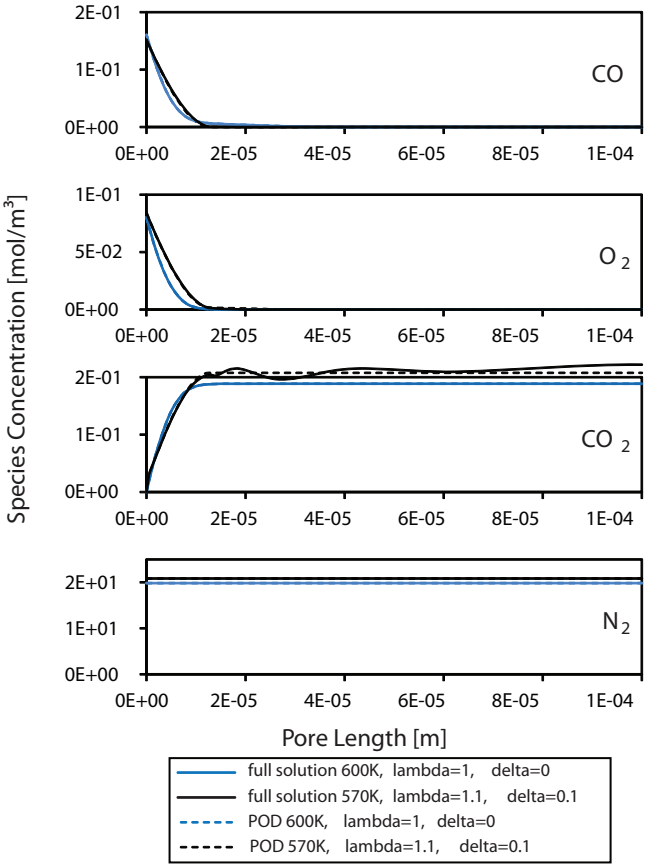

Figure 5. Comparison between full model solution and POD results for gas-phase species.

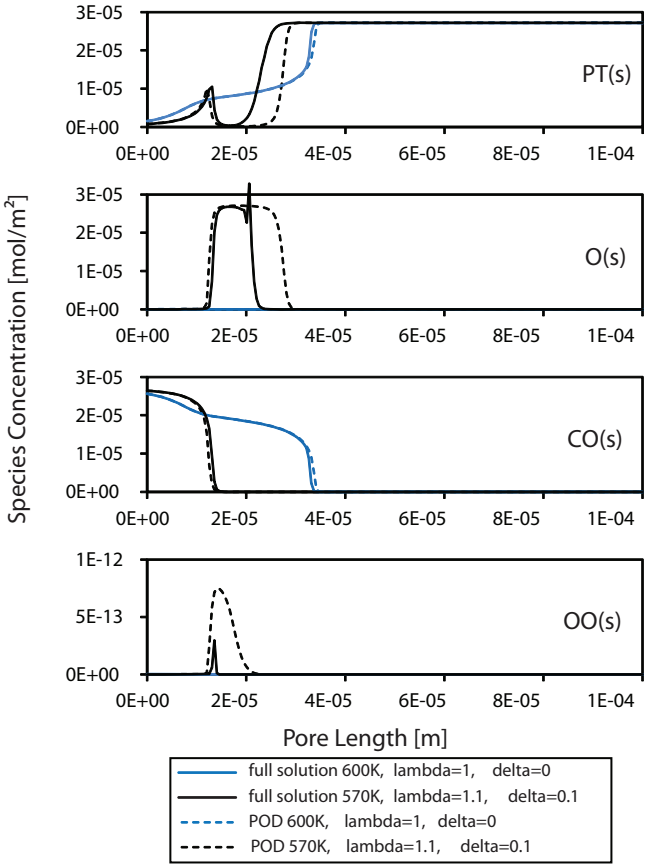

Figure 6. Comparison between full model solution and POD results for solid species.

for the evaluation of the ROM-Jacobian. The output log of the ODE integrator (MATLAB's ode15s) shown in Table 5 offers further insight into the possible reasons for this behaviour.

In some respects the ROM appears easier to solve than the full model, requiring around 37 % less time, 62 % fewer evaluations of the right-hand-side as well as 62 % fewer linear system solves. This, however, is offset by an only modest saving of 18 % in Jacobian evaluations and 37 % in LU decompositions. In essence, this is due to the ratio n/N of the sizes of reduced and full model, which is too large to compensate the increased cost of the dense computations (Table 6).

The relatively good performance of the full problem also benefits from a tuning of the parameters for the ODE solver, for example separate absolute and relative error tolerances for each species and the use of the non-negative option. This requires deep insight into the structure of the problem, especially in the structure of the chemical source term. This a priori information is not available for the ROM, so standard values have to be used for the ODE solver instead. In addition, and more importantly, the non-negative option cannot be used (the components of the POD solution can be negative), so the control over the non-negativity of the species is lost. It should be mentioned that, without the parameter tuning, the full problem performed considerably worse than the ROM. All these effects combined lead to the somewhat disappointing performance of the ROM in this particular case.

Table 5. Performance comparison at different conditions using a base from 600 K, $\lambda = 1$ and $\delta = 0$

Input value			Timing full system [s]	Timing reduced system [s]	Ratio reduced/full
T in K	λ	δ			
600	1.0	0	6.01	6.23	1.04
600	0.9	0	5.29	4.42	0.84
600	1.1	0	2.07	1.42	0.69
600	1.0	0.1	4.02	3.59	0.89
600	1.0	0.2	3.72	3.43	0.92
600	1.0	0.3	6.30	7.77	0.98
570	1.0	0	5.77	6.23	1.08
630	1.0	0	2.96	2.93	0.99
600	0.9	0.1	4.56	3.80	0.83
600	1.1	0.1	1.97	1.70	0.86
630	1.1	0.1	1.59	1.26	0.79
570	0.9	0.1	6.70	4.39	0.65
570	1.1	0.1	2.68	2.17	0.81

Table 6. Log of the ODE integrator

	Full problem	POD ROM
ODE steps	1369	463
Failed attempts	309	215
Function evaluations	3411	1307
Computed Jacobians	165	135
LU decompositions	508	320
Solutions of linear system	3408	1305

CONCLUSION AND OUTLOOK

The model reduction method of POD was applied to a reaction-diffusion problem exemplary for automotive exhaust-gas aftertreatment systems. However, the method investigated is not restricted to this application. The methodology is expected to be applicable to other systems where reaction-diffusion processes in pores are relevant, for example biomass or coal conversion.

It was shown that the method can be successfully applied to systems with complex non-linear source terms. The POD basis was obtained for each involved species separately using an individual number of basis vectors based on an error criterion. This was necessary due to the characteristic differences in species concentrations and dynamics in this kind of stiff reaction-diffusion system. Using a POD basis calculated for one baseline case, predictions for other temperature and species concentrations could be made.

The solutions obtained from the reduced system were comparable to the solutions obtained from solving the full system with respect to computing time and accuracy. However, the observed time savings were not as significant as reported for other applications. This is suspected to be due to the additional matrix multiplications introduced by the transformation of the non-linear source terms.

In future work, the calculation speed and accuracy of the ROM will be further investigated. Further gains in efficiency of the ROM were observed using the DEIM to accelerate the evaluation of the nonlinearity. Another interesting topic could be the influence of the used grid on the POD parameters. Using a fine grid initially and switching to a coarser one when possible could decrease computational speed without significant loss in accuracy.

NOMENCLATURE

C	concentration
k_k	rate coefficient of reaction
$\dot{S}_i$	reaction rate
t	time
X	pore length
A_k	pre-exponential factor
$D_{\mathrm{eff},i}$	effective diffusion coefficient
$D_{\mathrm{knud},i}$	Knudsen diffusion coefficient
$D_{\mathrm{mol},i}$	molecular diffusion coefficient
$E_{\mathrm{a,k}}$	activation energy
K_S	number of surface reactions
N_{G}, N_{S}	number of gas-phase/surface species
R	universal gas constant
S_i^0	sticking coefficient
T	temperature
W	molecular weight

Greek Symbols

β_{k}	temperature exponent
γ	catalytic active surface area per washcoat volume
δ	conversion factor
ε	porosity
λ	equivalence ratio
μ_{ik}, $\in_{ik}$	parameters for surface species interaction
ν'_{ik}, ν''_{ik}	stoichiometric coefficient of forward/backward reaction
$\tilde{\nu}'_{ik}$	reaction order of species j in reaction k
σ_i	number of occupied surface spots
τ	tortuosity
Γ	surface site density
Θ_i	surface coverage fraction

ACKNOWLEDGEMENTS

This research has been funded by the Saxon Ministry of Science and Fine Arts and the European Union in the project BioRedKat – Verbrennungstechnische Eigenschaften und deren Auswirkung auf die katalytische Schadstoffreduktion von biogenen flüssigen Energieträgern (project number 100097882) and by the Federal Ministry of Education and Research of Germany in the framework of Virtuhcon (project number 03Z2FN11). The third author was funded by the European Social Fund and State of Saxony grant 995.319570.6.

REFERENCES

[1] G. C. Koltsakis, P. A. Konstantinidis, A. M. Stamatelos, *Appl. Catal., B* **1997**, *12*, 161.

[2] K. Ramanathan, C. S. Sharma, *Ind. Eng. Chem. Res.* **2011**, *50*, 9960.

[3] R. Holder, *A Global Reaction Mechanism for Transient Simulations of Three-Way Catalytic Converters*, PhD Thesis, RWTH Aachen University, Aachen, Germany 2008.

[4] E. S. J. Lox, *Handbook of Heterogeneous Catalysis*, 2nd Edition, Wiley-VCH Verlag GmbH & Co. KGaA, Weinheim **2008**, p. 2274.

[5] R. M. Heck, R. J. Farrauto, *Appl. Catal., A* **2001**, *221*, 443.

[6] F. Keil, *Catal. Today* **1999**, *53*, 245.

[7] P. Kočí, V. Novák, F. Štěpánek, M. Marek, M. Kubíček, *Chem. Eng. Sci.* **2010**, *65*, 412.

[8] P. Kočí, M. Kubíček, M. Marek, *Ind. Eng. Chem. Res.* **2004**, *43*, 4503.

[9] R. J. Kee, M. E. Coltrin, P. Glarborg, *Chemically Reacting Flow*, 1st edition, John Wiley & Sons, Hoboken, USA **2003**, p. 452.

[10] M. Dadvar, M. Sahimi, *Chem. Eng. Sci.* **2007**, *62*, 1466.

[11] O. Deutschmann, *Interactions Between Transport and Chemistry*, Ruprechts-Karl Universität Heidelberg, Heidelberg, Germany **2001**, p. 29.

[12] N. Mladenov, J. Koop, S. Tischer, O. Deutschmann, *Chem. Eng. Sci.* **2010**, *65*, 812.

[13] W. Edelbauer, S. Kutschi, J. C. Wurzenberger, *SAE Int. J. Engines* **2012**, *5*, 1459.

[14] B. A. Grzybowski, *Chemistry in Motion*, 1st edition, John Wiley & Sons, Chichester, UK **2009**, p. 61.

[15] L. F. Shampine, M. W. Reichelt, *SIAM J. Sci. Comput.* **1997**, *18*, 1.

[16] G. Leofanti, M. Padovan, G. Tozzola, B. Venturelli, *Catal. Today* **1998**, *41*, 207.

[17] J. Rouquerol, D. Avnir, C. W. Fairbridge, D. H. Everett, J. M. Haynes, N. Pernicone, J. D. F. Ramsay, K. S. W. Sing, K. K. Unger, *Pure Appl. Chem.* **1994**, *66*, 1739.

[18] R. E. Hayes, S. T. Kolaczkowski, *Introduction to Catalytic Combustion*, Gordon & Breach, Amsterdam **1997**, p. 245.

[19] O. Deutschmann, H. Knözinger, K. Kochloefl, T. Turek, "Heterogeneous Catalysis and Solid Catalysts, 1.

Fundamentals," *Ullmann's Encyclopedia of Industrial Chemistry*, Wiley-VCH Verlag GmbH & Co. KGaA, Weinheim **2009**, p. 477.

[20] S. Salomons, R. E. Hayes, M. Votsmeier, A. Drochner, H. Vogel, S. Malmberg, J. Gieshoff, *Appl. Catal., B* **2007**, *70*, 305.

[21] P. Holmes, J. L. Lumley, G. Berkooz, C. W. Rowley, *Turbulence, Coherent Structures, Dynamical Systems and Symmetry*, 2nd edition, Cambridge University Press, Cambridge **2012**, p. 68.

[22] W. Jürgens, H.-J. Kaltenbach, *J. Turbul.* **2003**, *4*, N18.

[23] M. Voisine, L. Thomas, J. Borée, P. Rey, *Exp. Fluids* **2010**, *50*, 1393.

[24] H. Chen, D. L. Reuss, D. L. Hung, V. Sick, *Int. J. Engine. Res.* **2012**, *14*, 307.

[25] H. M. Park, D. H. Cho, *Int. J. Heat Mass Transfer* **1996**, *39*, 3311.

[26] M. D. Graham, I. G. Kevrekidis, *Comput. Chem. Eng.* **1996**, *20*, 495.

[27] G. H. Golub, C. F. Van Loan, *Matrix Computations*, 3rd edition, Johns Hopkins University Press, Baltimore **1996**.

[28] M. Buffoni, K. Willcox, "Projection-based model reduction for reacting flows," *40th Fluid Dynamics Conference and Exhibit*, Chicago, USA, 28 June–1 July **2010**.

[29] S. Chaturantabut, D. C. Sorensen, "Discrete Empirical Interpolation for nonlinear model reduction," *Proc. 48h IEEE Conference on Decision and Control*, Shanghai, China, 15–18 December **2009**, p. 4316.

Manuscript received August 31, 2013; revised manuscript received February 20, 2014; accepted for publication February 25, 2014.